Phase Diagram for the Breakdown of the Quantum Hall Effect

L. B. Rigal, D. K. Maude, M. Potemski, and J. C. Portal
Grenoble High Magnetic Field Laboratory, Max Planck Institut für Festkörperforschung and Centre National de la Recherche Scientifique, BP 166, 38042 Grenoble Cedex 9, France

L. Eaves
Department of Physics, University of Nottingham, Nottingham NG7 2RG, United Kingdom

Z. R. Wasilewski
Institute for Microstructural Sciences, National Research Council, Ottawa, Canada, K1A 0R6

G. Hill and M. A. Pate
Department of Electronic and Electrical Engineering, University of Sheffield, Sheffield S1 4DU, United Kingdom
(Received 5 June 1998)

The breakdown of the dissipationless conductance in the integer quantum Hall effect regime has been investigated over a wide range of filling factors. The temperature dependence of the critical current and of the critical magnetic field at breakdown bears a striking resemblance to the phase diagram of the phenomenological two-fluid Gorter-Casimir model for superconductivity. [S0031-9007(99)08459-8]

PACS numbers: 73.40.Hm, 71.10.Pm, 74.25.Dw

The breakdown of the integer quantum Hall effect (IQHE) has been extensively investigated [1–5] with most work concentrating on the sample width and magnetic field (filling factor) dependence of the critical current required to destroy the dissipationless conductance at integer filling factors. An understanding of the physical origin of breakdown and its implications for the resistance standard are of fundamental importance [3]. From a theoretical point of view a number of models have been proposed [6–11] but the exact mechanism for the breakdown remains controversial. What is clear is that the breakdown is driven by the Hall voltage $V_H = I \frac{h}{\nu e^2}$ for a current I at integer filling factor ν. In addition, for the rather high critical currents typically observed, the current flows through both edge states and the bulk of the sample [5,12].

In this Letter we show that it is possible to map out a phase diagram (critical current or critical magnetic field versus temperature) for the breakdown of the IQHE. The measured phase diagram for different filling factors is all related by a remarkably simple scaling law. Perhaps more surprising is the striking resemblance to the phase diagram for the coercive field in a superconductor. This is unexpected since there is currently no theoretical basis to connect the IQHE and superconductivity. Theoretical work has been limited to linking the fractional quantum Hall effect (FQHE) to superconductivity [13–16], although it has been suggested that in sufficiently narrow quantum Hall systems it should be possible to observe Josephson-type oscillations in the IQHE regime [17,18].

For the investigation a series of modulation doped 8.2 nm single quantum well structures was grown by molecular beam epitaxy. Hall bars were patterned to have a width $d = 250$ with 750 μm between voltage probes. The mobility ranged from 3–22 $m^2 V^{-1} s^{-1}$ for carrier densities of (6–14) $\times 10^{11}$ cm^{-2}. Results for even filling factors on only one sample are shown for reasons of space but all of the samples investigated showed the same behavior.

A typical magnetoresistance trace measured at 2.0 K is shown in Fig. 1(a) for a sample cooled slowly and in the dark to obtain a carrier density of 7.28×10^{11} cm^{-2} and a mobility of 11 $m^2 V^{-1} s^{-1}$. The critical current (I_c) was determined by measuring four terminal I-V

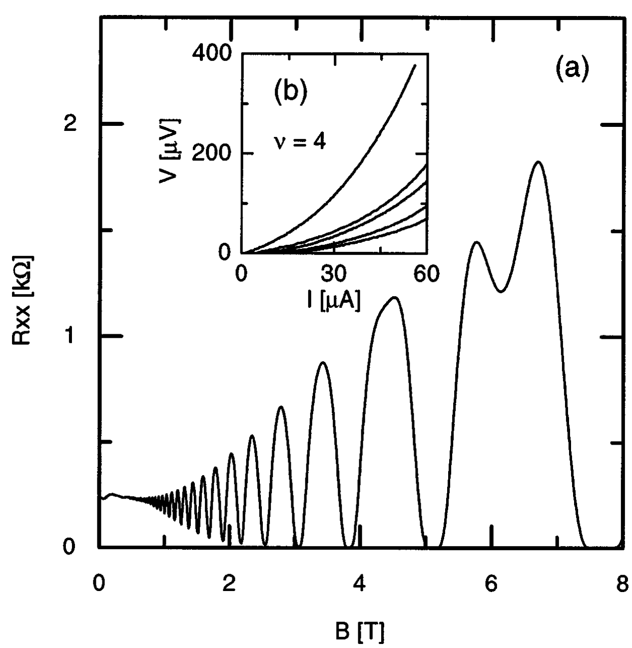

FIG. 1. (a) Magnetoresistance measured at $T = 2.0$ K. (b) Current-voltage characteristics measured at $B = 7.7$ T ($\nu = 4$) for temperatures 2–6 K.

characteristics for magnetic fields at 10 mT intervals in such a way as to sweep through the particular filling factor. A plot of I_c versus magnetic field gives a slightly asymmetric Gaussian (not shown) with the maximum corresponding to the magnetic field for which ν is an integer. The critical current for a given filling factor is taken to be the maximum of the Gaussian. Representative I-V characteristics measured at 7.70 T corresponding to the field for the maximum I_c are shown in Fig. 1(b) for different temperatures in the range 2–6 K.

For a given sample I_c is dependent on the pair of voltage contacts chosen, the sign of the current, and the magnetic field direction. Contacts which have a high critical current show a very abrupt increase in voltage upon breakdown which, we believe, is due to an avalanche heating process. While such contacts have the advantage that the critical current is well defined they have the major drawback that the large currents involved can lead to heating in the current contacts. This can be easily identified during the measurements due to the large voltage drop across the current contacts and a noticeable heating of the temperature sensor even for currents for which the conductance between the voltage contacts under study remains dissipationless. Therefore, we choose contacts for which I_c is sufficiently small to avoid Ohmic heating in the current contacts. Throughout the measurements I_c has been defined as the current for which the measured voltage between the voltage probes exceeds 50 μV. The value of I_c is therefore somewhat arbitrary but we have verified that, although choosing different critical voltages changes the absolute value of I_c, it does not in any way modify the form of the temperature dependence or the scaling between different filling factors.

The temperature dependence of I_c is shown in Fig. 2(a). For a given filling factor I_c has an almost constant value at low temperatures before decreasing and then vanishing at a critical temperature (T_c). The resemblance to the phase diagram for the coercive field of a superconductor is striking (for superconductors I_c and H_c are equivalent since the superconductivity is also quenched when the current is sufficient to produce its own critical magnetic field). The solid lines are generated using an expression similar to that for the phenomenological Gorter-Casimir [19] two-fluid model for superconductivity,

$$I_c(T,\nu) = \left(\frac{I_{c0}}{\nu} - \frac{I_{c0}}{\nu_0}\right)\left[1 - \left(\frac{T}{T_{c0}/\nu}\right)^2\right], \quad (1)$$

where $I_{c0} = 314$ μA and $\nu_0 = 30$ are obtained from the straight line fit to $I_c(T \sim 0)$ versus $1/\nu$ shown in Fig. 2(b). The value of ν_0 has the physical significance that this is the largest filling factor for which the conduction is expected to be dissipationless at zero temperature. From the magnetic field, at which Shubnikov–de Haas oscillations are first observed, this corresponds to the condition $\omega_c \tau \approx 2$. The only remaining parameter

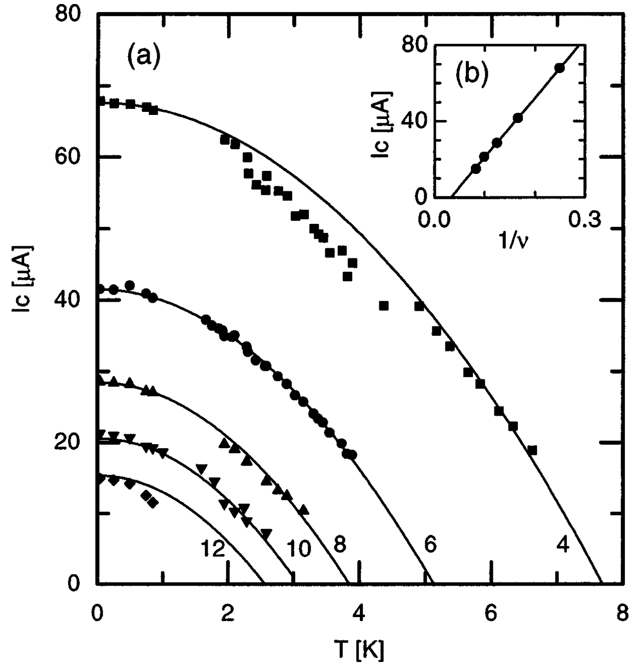

FIG. 2. (a) Critical current (I_c) as a function of temperature for even filling factors. The solid lines are calculated using Eq. (1) as described in the text. (b) I_c(40 mK) versus inverse filling factor ($1/\nu$). The solid line is a least squares fit to the data.

$T_{c0} = 31$ K is found by fitting Eq. (1) to the temperature dependence of I_c for the filling factor $\nu = 6$. The temperature dependence of I_c can then be generated using Eq. (1) for the other filling factors with no adjustable parameters. The agreement between the data and the model for all filling factors is remarkable and an equally good agreement has been found in all samples. The critical current and the critical temperature scale as the cyclotron energy ($\hbar\omega_c \propto 1/\nu$). The critical Hall electric field at $T = 0$, $F_c = \frac{I_c}{d}\frac{h}{\nu e^2} \simeq \frac{32\,400}{\nu^2}(1 - \frac{\nu}{\nu_0}) \approx 1800$ V/m for $\nu = 4$. This gives a B dependence not dissimilar to that reported for narrower Hall bar samples [2].

We now turn our attention to the temperature dependence of the width of the dissipationless regions in the magnetoresistance traces. Pursuing the analogy with the Gorter-Casimir model, we will try to map out a B_c versus T phase diagram for the different filling factors. Magnetoresistance traces were measured at different temperatures and with a small current $\simeq 10$–100 nA using low frequency (10.7 Hz) phase sensitive detection. B_c is defined as the half-width of the dissipationless region at each filling factor. In order to determine the width of the dissipationless region we define a critical sample resistance $R_c \simeq 10$ Ω which is approximately 5% of the zero field resistance. Choosing different values for R_c changes the absolute value of B_c but in no way modifies the form of the temperature dependence.

Such a phase diagram for even integer filling factors is shown in Fig. 3(a). At first sight the data points bear

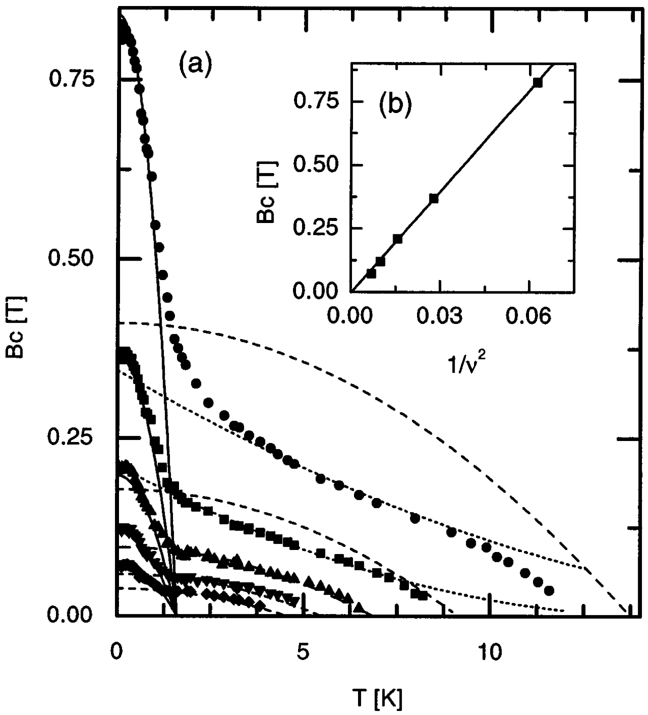

FIG. 3. (a) Critical magnetic field (B_c) versus temperature for even filling factors ($\nu = 4$, 6, 8, 10, and 12) clearly showing the existence of two phases. The dashed (HT phase), solid (LT phase), and dotted (melting) lines are calculated using Eqs. (2)–(4), respectively. (b) B_c(40 mK) versus $1/\nu^2$. The solid line is a least-squares fit to the data.

little resemblance to the Gorter-Casimir phase diagram. However, as indicated by the solid and dashed lines, it is possible to decompose this phase diagram into a low temperature (LT) and high temperature (HT) phase. The HT phase can be fitted using

$$B_c(\nu,T) = \left(\frac{B_{c0}^{\mathrm{HT}}}{\nu^2} - \frac{B_{c0}^{\mathrm{HT}}}{\nu_0^2}\right)\left[1 - \left(\frac{T}{T_{c0}^{\mathrm{HT}}/\nu}\right)^2\right], \quad (2)$$

where $\nu_0 = 30$ (as before) and $B_{c0}^{\mathrm{HT}} = 6.7$ T and $T_{c0}^{\mathrm{HT}} = 54$ K are determined by fitting to the data for $\nu = 8$. The curves for all the other filling factors [dashed lines in Fig. 3(a)] are then generated using Eq. (2) with no adjustable parameters. For $\nu = 8$, 10, and 12 the agreement is good while for lower filling factors there is a deviation with the data dipping below the predicted curve for a substantial part of the phase diagram.

The LT phase in Fig. 3(a) can be fitted using

$$B_c(\nu,T) = \left(\frac{B_{c0}^{\mathrm{LT}}}{\nu^2} - \frac{B_{c0}^{\mathrm{LT}}}{\nu_0^2}\right)\left[1 - \left(\frac{T}{T_{c0}^{\mathrm{LT}}}\right)^2\right], \quad (3)$$

which is identical to Eq. (2) except that $T_c = T_{c0}^{\mathrm{LT}}$ no longer scales as the cyclotron energy, i.e., in the LT phase the critical temperature is the same for all filling factors. In contrast to the behavior of $I_c(T \sim 0)$, for both the LT and HT phases, $B_c(T \sim 0)$ scales as the cyclotron energy squared ($1/\nu^2$) as shown in Fig. 3(b). From the slope $B_{c0}^{\mathrm{LT}} = 13.4$ T. The solid lines in Fig. 3(a) are generated by fitting to the low temperature $\nu = 4$ data to determine $T_{c0}^{\mathrm{LT}} = 1.6$ K with $\nu_0 = 30$ as before.

B_c is determined simply by the number of localized states in the relevant Landau level (LL). It is easy to show that the normalized density of localized states in the LL $n_{\mathrm{loc}}/n_{\mathrm{LL}} = 2\nu B_c/B_F \sim 20\%$ for $\nu = 4$ at $T \sim 0$ with the fundamental field $B_F = 30.3$ T. As $B_c \propto 1/\nu^2$ this implies that the density of localized states within a LL is proportional to the magnetic field ($\propto 1/\nu$). I_c, which is determined with the Fermi level centered in the localized states between LLs is apparently insensitive to the exact number of delocalized states since only one phase is observed. It is not clear why two phases are observed for B_c but this must be linked to increased localization at low temperatures, possibly associated with the critical appearance of spin splitting [20,21]. To our knowledge no detailed calculations for the number of localized states in a LL and its dependence on filling factor exist. At odd filling factors (not shown) only one phase is observed which supports the link to spin splitting, since the LL to be populated is separated from the next unoccupied LL by the cyclotron energy and therefore only one spin state is occupied. However, for even filling factors two phases are present even in low mobility samples in which no spin splitting is observed.

We noted above that for lower filling factors in Fig. 3 the data dips below the high temperature fitting curve for a substantial part of the phase diagram. A similar deviation is observed in the phase diagram of high temperature (HT_c) superconductors and is associated with the melting curve of the Abrikosov vortex lattice [22]. In the liquid phase, when a current is applied, the vortices are free to move under the influence of the Lorentz force which leads to dissipation and the superconductivity is quenched. In type-II superconductors the critical field can be enhanced by the addition of impurities which pin the vortices and prevent flux jumping, while in the QHE disorder increases the number of localized states and hence enhances B_c. For the IQHE the "melting" would correspond to a delocalization of cyclotron orbit centers. We therefore make an analogy with type-II superconductors and, in particular, HT_c superconductors with a weak interlayer coupling which show a 2D behavior. The melting behavior suggested by the deviation of the data points from Eq. (2) can be fitted to the functional form of the Abrikosov lattice melting curve,

$$B_c(\nu,T) = \left(\frac{B_m}{\nu} - \frac{B_m}{\nu_0}\right)\left(1 - \frac{T}{T_m/\nu}\right)^2. \quad (4)$$

A good fit for the lower ν values can be obtained with $B_m = 1.6$ T, $\nu_0 = 30$, and $T_m = 90$ K. Here the $1/\nu$ scaling law has been determined empirically. The predicted melting curves for $\nu = 8$, 10, and 12 (not shown) lie above the usual phase boundary and hence these filling factors are unaffected. For $\nu = 6$, the data follow the melting curve to join the HT phase near T_c while for $\nu = 4$, the data dip below the melting curve close to the predicted T_c and appears to have a critical temperature ~ 2 K lower than expected. This is similar to the Berezinskii-Kosterlitz-Thouless (BKT) behavior observed in 2D superconductors [22–25] due to intrinsic vortex-antivortex excitations which destroy the topological order and lead to a critical temperature T_{BKT} which is typically ~ 1 K less than T_c. Although the comparison of the HT_c and QHE phase diagrams is clearly intriguing such an interpretation of our data would be speculative.

An interpretation of the above findings, in particular, with respect to the analogy with superconductivity, necessarily requires detailed theoretical work. The analogy between the dissipationless conductance in the FQHE and superconductivity has been discussed in a number of theoretical papers [13–15]. Girvin and MacDonald [13] proposed an effective-field-theory model analogous to the Landau-Ginzburg theory of superconductivity in which the FQHE can be viewed as a superconducting state of composite bosons. Aronov and Mirlin [16] demonstrated that the low temperature conductivity of such an anyon gas in the presence of impurity scattering remains finite but tends exponentially towards zero with decreasing temperature. Invoking a gauge transformation to form composite bosons and associated anyon superconductivity would seem difficult to justify since the IQHE is well explained without taking into account electron-electron interactions. In our opinion the similarity between the phase diagrams arises from the similarity of the Hamiltonians: the vortex term in the Hamiltonian of a 2D superconductor is identical to that of Coulomb gas in two dimensions [22].

In conclusion, the phase diagram for the breakdown of the IQHE is well described phenomenologically by the equations of the two-fluid model for superconductivity. It exhibits a remarkably simple scaling law for the different filling factors. The similarity between the HT_c and QHE phase diagrams is a striking one. We hope that the results presented here will stimulate further work, in particular, concerning the possible analogy between superconductivity and the IQHE. In addition it would seem interesting to investigate the phase diagram for the breakdown of the FQHE for which a certain amount of theory already exists.

[1] G. Ebert, K. von Klitzing, K. Ploog, and G. Weimann, J. Phys. C **16**, 5441 (1983).
[2] S. Kawaji, Semicond. Sci. Technol. **11**, 1546 (1996), and references therein.
[3] M. E. Cage, R. F. Dziuba, B. F. Field, E. R. Williams, S. M. Girvin, A. C. Gossard, D. C. Tsui, and R. J. Wagner, Phys. Rev. Lett. **51**, 1374 (1983).
[4] P. M. Mensz and D. C. Tsui, Phys. Rev. B **40**, 3919 (1989).
[5] N. Q. Balaban, U. Meirav, H. Shtrikman, and Y. Levinson, Phys. Rev. Lett. **71**, 1443 (1993); N. Q. Balaban, U. Meirav, and H. Shtrikman, Phys. Rev. B **52**, R5503 (1995).
[6] S. Komiyama, T. Takamasu, S. Hiyamizu, and S. Sasa, Solid State Commun. **54**, 479 (1985).
[7] O. Heinonen, P. L. Taylor, and S. Girvin, Phys. Rev. B **30**, 3016 (1984).
[8] L. Eaves and F. W. Sheard, Semicond. Sci. Technol. **1**, L346 (1986).
[9] S. A. Trugman, Phys. Rev. B **27**, 7539 (1983).
[10] K. Ishikawa, N. Maeda, and K. Tadaki, Phys. Rev. B **54**, 17 819 (1996)
[11] V. Tsemekhman, K. Tsemekham, C. Wexler, J. H. Han, and D. J. Thouless, Phys. Rev. B **55**, R10 201 (1997).
[12] K. von Klitzing, Physica (Amsterdam) **184B**, 1 (1993).
[13] S. M. Girvin and A. H. MacDonald, Phys. Rev. Lett. **58**, 1252 (1987)
[14] R. B. Laughlin, Phys. Rev. Lett. **60**, 2677 (1988).
[15] S. C. Zhang, T. H. Hansson, and S. Kivelson, Phys. Rev. Lett. **62**, 82 (1989).
[16] A. G. Aronov and A. D. Mirlin, Phys. Lett. A **152**, 371 (1991).
[17] Y. Imry, Physica (Amsterdam) **152B**, 295 (1988).
[18] V. Srivastava, Physica (Amsterdam) **212B**, 299 (1995).
[19] C. J. Gorter and H. B. G. Casimir, Physica (Utrecht) **1**, 306 (1934).
[20] M. M. Fogler and B. I. Shklovski, Phys. Rev. B **52**, 17 366 (1995).
[21] D. R. Leadley, R. J. Nicholas, J. J. Harris, and C. T. Foxon, Phys. Rev. B **58**, 13 036 (1998).
[22] G. Blatter, M. V. Feigel'man, V. B. Geshkenbein, A. I. Larkin, and V. M. Vinokur, Rev. Mod. Phys. **66**, 1125 (1994), and references therein.
[23] J. M. Kosterlitz and D. J. Thouless, J. Phys. C **6**, 1181 (1973).
[24] S. Martin, A. T. Fiory, R. M. Fleming, G. P. Espinosa, and A. S. Cooper, Phys. Rev. Lett. **62**, 677 (1989).
[25] J. C. Garland and Hu Jong Lee, Phys. Rev. B **36**, 3638 (1987).